PHYSICAL REVIEW E **89**, 052505 (2014)

# Shape-dependent dispersion and alignment of nonaggregating plasmonic gold nanoparticles in lyotropic and thermotropic liquid crystals

Qingkun Liu,[1] Jianwei Tang,[2] Yuan Zhang,[1,2] Angel Martinez,[1] Shaowei Wang,[2] Sailing He,[2] Timothy J. White,[3] and Ivan I. Smalyukh[1,4,5,*]

[1]*Department of Physics and Materials Science and Engineering Program, University of Colorado at Boulder, Boulder, Colorado 80309, USA*

[2]*Centre for Optical and Electromagnetic Research, Zhejiang University, Hangzhou 310058, People's Republic of China*

[3]*Air Force Research Laboratory, Materials and Manufacturing Directorate, WPAFB, OH, USA*

[4]*Department of Electrical, Computer, and Energy Engineering and Liquid Crystals Materials Research Center, University of Colorado at Boulder, Boulder, Colorado 80309, USA*

[5]*Renewable and Sustainable Energy Institute, National Renewable Energy Laboratory and University of Colorado, Boulder, Colorado 80309, USA*

(Received 17 April 2014; published 15 May 2014)

We use both lyotropic liquid crystals composed of prolate micelles and thermotropic liquid crystals made of rod-like molecules to uniformly disperse and unidirectionally align relatively large gold nanorods and other complex-shaped nanoparticles at high concentrations. We show that some of these ensuing self-assembled orientationally ordered soft matter systems exhibit polarization-dependent plasmonic properties with strongly pronounced molar extinction exceeding that previously achieved in self-assembled composites. The long-range unidirectional alignment of gold nanorods is mediated mainly by anisotropic surface anchoring interactions at the surfaces of gold nanoparticles. Polarization-sensitive absorption, scattering, and extinction are used to characterize orientations of nanorods and other nanoparticles. The experimentally measured unique optical properties of these composites, which stem from the collective plasmonic effect of the gold nanorods with long-range order in a liquid crystal matrix, are reproduced in computer simulations. A simple phenomenological model based on anisotropic surface interaction explains the alignment of gold nanorods dispersed in liquid crystals and the physical underpinnings behind our observations.

DOI: 10.1103/PhysRevE.89.052505 PACS number(s): 83.80.Xz, 78.67.Bf, 81.05.Xj, 81.16.Dn

## I. INTRODUCTION

The assembly of microparticles and nanoparticles into a variety of mesoscopic architectures has gained much attention due to the novel effect of their long-range order on their optical and electronic properties [1–18]. Liquid crystals (LCs) are promising fluidic hosts to assemble nanoparticles. LCs can organize the dispersed particles in various ways based on different mechanisms, depending on the particle size, shape, and surface treatment. The organization of diverse anisometric nanoparticles, such as gold nanorods (GNRs), carbon nanotubes, and magnetic nanoparticles, into different spatial patterns in LCs has been achieved in different LC systems [10,19–27]. This recent work significantly expands the research efforts on forming LC composites, often utilizing molecular dyes and LCs as a host medium [28]. One of the well-known issues is that the dyes, typically containing large aromatic molecular groups, are rather chemically unstable [28]. The significant progress in the concentrated dispersion and alignment of anisotropic nanoparticles with diameters of 20 nm and larger may open a new possibility of using anisotropic nanoparticles instead of dyes. However, stable self-organization of nonaggregating nanocolloids of comparably larger sizes in LCs remains a challenging task because the colloids disturb the LC director field, which results in elastic interparticle forces and ensuing aggregation. Here, we overcome this challenge through accomplishing relatively weak surface anchoring at the LC-nanoparticle interfaces, including mesomorphic fluid host systems of both lyotropic and thermotropic types.

In this work, we describe the concentrated dispersion of gold nanoparticles of different shapes and sizes as well as the spontaneous unidirectional self-alignment of relatively large GNRs in lyotropic and thermotropic LC matrices. This nematic-like alignment of GNRs is characterized by polarization-dependent extinction and scattering properties. Different alignment methods including shear force, confinement, and light reorientation of photoalignment systems are utilized to align GNRs that follow the liquid crystal director. The oriented self-assembly of GNRs at high concentrations gives rise to novel optical properties of the composite medium, such as unusual dispersions of refractive index and enhanced optical birefringence with sign reversal at the longitudinal surface plasmon resonance (SPR) peak. We use a simple physical model based on the anisotropic surface anchoring interactions to explain behavior and properties of GNRs in nematic LCs of both lyotropic and thermotropic types. This work, demonstrating nematic-mediated orientational ordering of GNRs with positive scalar orientational order parameter, is partially complementary to our recent paper [20], in which we have demonstrated a discotic nematic lyotropic system with negative order parameter of nematic-aligned GNRs at lower concentrations and of smaller size. Unique optical properties of self-assembled GNRs with long-range orientational ordering have the potential to be utilized in applications such as plasmonic polarizers.

*ivan.smalyukh@colorado.edu

 

## II. MATERIALS, METHODS, AND TECHNIQUES

### A. Dispersion of gold nanoparticles in lyotropic LCs

GNRs of various sizes were examined. Comparatively large, polymer coated GNRs (Nanopartz Inc.) with a mean diameter of 40 nm and mean length of 73 nm are used as supplied. Smaller GNRs with a mean diameter of 20 nm and mean length of 50 nm were synthesized according to Ref. [29]. Gold nanocubes and gold "nanostars" were synthesized according to Refs. [30,31], respectively. Gold nanoparticles are functionalized by thiol-terminated methoxy-poly(ethylene glycol) (mPEG-SH) for colloidal stability. The composite of mPEG-GNRs and lyotropic LC is prepared based on a ternary lyotropic LC of sodium decyl sulfate-decanol-water (SDS–1-decanol–water) with a known phase diagram [32]. A calamitic nematic ($N_C$) lyotropic LC was prepared using a composition of 37.5 wt% of SDS, 5.5 wt% of 1-decanol (both from Sigma-Aldrich), and 57.0 wt% of an aqueous suspension of mPEG-GNRs at $4.7 \times 10^{-8}$ M. This composition was centrifuged at 3000 rpm for 10 min and ultrasonicated for 30 min at room temperature to yield $N_C$ with rod-shaped micelles of about 2.6 nm in diameter and 6-nm long [33,34]. The concentrations of GNRs were verified using the known molar extinction coefficient at longitudinal SPR peak ($2.1 \times 10^{14}$ $M^{-1}cm^{-1}$) and the measured optical density. The final concentration of GNRs was about 4.8% by weight (~0.26% by volume) in $N_C$. The composite was injected into the LC cell and aligned by a unidirectional shear defining the far-field director $\mathbf{N_0}$.

### B. Dispersion of gold nanoparticles in thermotropic LCs

To disperse gold nanoparticles in a thermotropic LC, the mPEG-coated nanoparticles in an aqueous solution were redispersed into methanol via centrifuging at 9000 rpm for 20 min and washing by methanol three times. Fifty $\mu$L of GNRs in methanol was fully dried at 90° C for 1 h, followed by adding 15 $\mu$L of a nematic 4-cyano-4′-pentylbiphenyl (5CB, Chengzhi Yonghua Display Materials Co. Ltd.). Then the mixture was sonicated for 5 min at 40° C, yielding an excellent dispersion in the isotropic phase of 5CB. The isotropic GNPs-LC dispersion was cooled down to the nematic phase while vigorously stirring to mitigate the aggregation processes caused by the nucleation and growth of nematic domains within the isotropic melting. The composites were then centrifuged at 3000 rpm for 5 min to remove residual aggregates, yielding well-separated individual nanoparticles in LC. Droplets of gold nanoparticles-LC composites were dispersed in polydimethylsiloxane (PDMS). The unidirectional alignment of 5CB was achieved by rubbing spin-coated polyvinyl alcohol (PVA, 3000 rpm, 5 min) on glass by velvet cloth.

### C. Sample preparation and characterization

Photoalignment layers were obtained by spin-coating glass plates with a commercially available photoalignment mixture PAAD-22 (BEAM Co.) at 3000 rpm for 60 s [35] and baking it at 100 °C for 10 min. By illuminating the photoalignment layer with linearly polarized blue light of power ~50 $\mu$W for 5 min, $\mathbf{N_0}$ is set to be perpendicular to the linear polarization. This alignment persisted under ambient and imaging light, but could be controlled by varying the polarization of patterned blue-light illumination controlled on a pixel-by-pixel basis using a LC microdisplay with 1024 × 768 pixels (EMP-730, Epson) coupled to a microscope [36]. Polarizing and bright-field optical imaging of GNR-LC composites was performed using an Olympus BX-51 upright polarizing optical microscope (POM) with 10 ×, 20 ×, and 50 × dry objectives (all from Olympus) with numerical aperture within 0.3–0.9 and a CCD camera (Spot 14.2 Color Mosaic, Diagnostic Instruments, Inc.). Polarization-dependent extinction spectra were obtained using a spectrometer (USB2000-FLG, Ocean Optics) mounted on an optical microscope, right behind a linear polarizer. Dark-field microscopy was performed using the same microscope equipped with an oil-immersion dark-field condenser (numerical aperture of 1.2) and a polarizer in the optical path in front of the camera; only highly scattered light was collected using a 20 × air objective.

## III. RESULTS

### A. Dispersion and alignment

One of the unique features of the dispersion of nonspherical nanoparticles in LCs is that they tend to spontaneously align with respect to the LC director **N**, which can be illustrated with the example of rod-like particles such as GNRs. The schematics of the nanostructured assembly of GNRs in lyotropic and thermotropic nematic LC shown in Figs. 1(a)–1(d) are based on the analysis of polarization-dependent extinction spectra, POM, and polarized dark-field scattering images. The nematic director **N** describes the local average orientation of long axis of prolate micelles [Fig. 1(a)] or rod-shaped 5CB molecules [Fig. 1(b)] forming the LC phase. The orientation of the long axes of GNRs are, on average, parallel to **N** [Fig. 1(c)] and the assembled GNRs in a nematic phase with a far field director $\mathbf{N_0}$ form a plasmonic complex fluid, which exhibits long-range orientational ordering [Fig. 1(d)].

mPEG-capped gold nanoparticles without a well-pronounced anisotropy of shapes like nanocubes and "nanostars" can be also dispersed in LC hosts like 5CB without aggregation. The mPEG on the surface of gold nanopaticles gives rise to weak tangential anchoring of 5CB on it, shown in

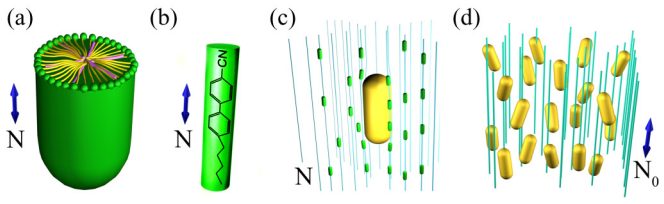


FIG. 1. (Color online) Schematic of (a) rod-like micelle of a ternary lyotropic LC and (b) chemical structure of the 5CB molecule with LC director **N** describing average orientation of their long axes. (c) Alignment of GNRs on average along the local director **N** describing average orientation of the rod-like micelles or 5CB molecules. (d) Oriented self-assembly of GNRs in a nematic LC, which exhibits long-range unidirectional ordering of rod-like nanoparticles along the far-field director $\mathbf{N_0}$.

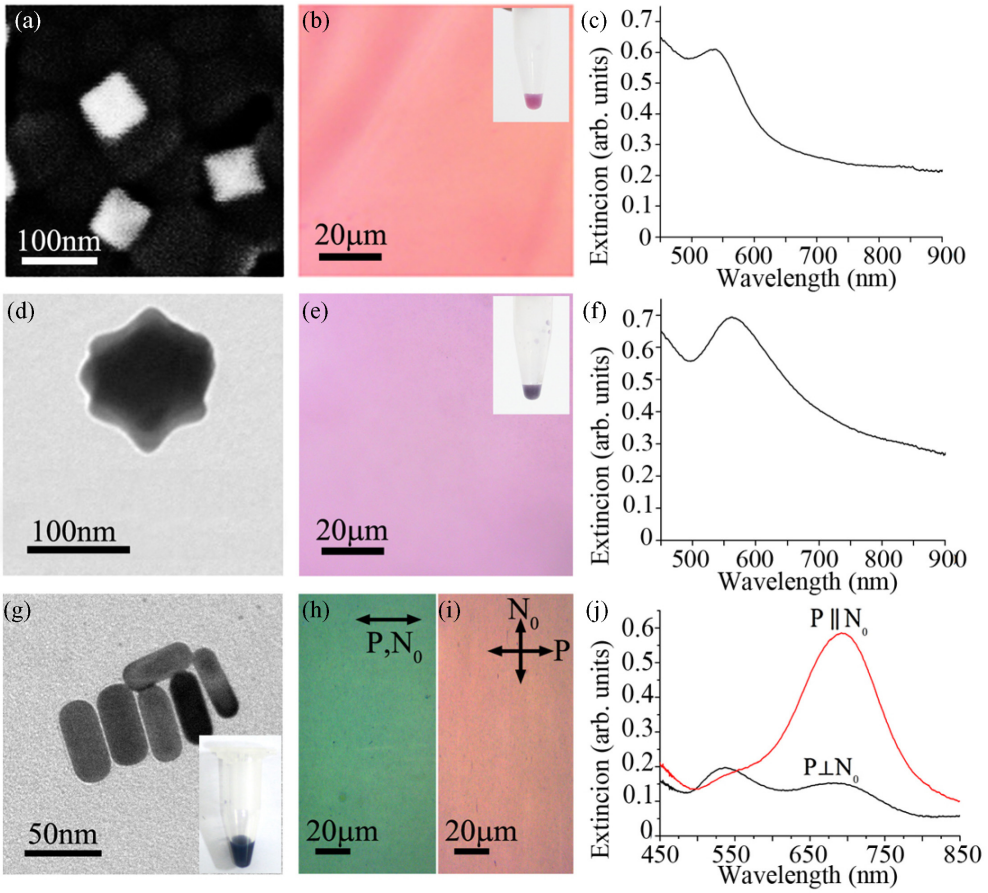


FIG. 2. (Color online) (a) SEM image of gold nanocubes. (b) Optical microscopy image of a dispersion of gold naoncubes in 5CB. The inset shows a vial with the gold nanocubes-5CB dispersion. (c) Polarization-independent extinction spectrum of gold nanocubes in 5CB. (d) Transmission electron microscopy (TEM) image of gold "nanostar." (e) Optical microscopy image of dispersion of gold "nanostars" in 5CB. The inset shows a vial with the gold "nanostars"-5CB dispersion. (f) Polarization-independent extinction spectrum of gold "nanostars" in 5CB. (g) TEM image of GNRs. The inset shows a vial with the GNRs-5CB dispersion. Transmission-mode optical images of GNRs-5CB sample with (h) $\mathbf{P}||\mathbf{N_0}$ and (i) $\mathbf{P}\perp\mathbf{N_0}$. (j) Polarization-dependent extinction spectra of GNRs-5CB sample.

Figs. 2(a), 2(b), 2(d), and 2(e). However, the high symmetry of nanoparticle shapes precludes their alignment, yielding practically polarization-independent extinction spectra of dispersions in the LC, see Figs. 2(c) and 2(f). However, GNRs are metallic nanoparticles that have strongly red-shifted longitudinal and transverse SPR modes polarized parallel to the long and short axes of the GNRs, respectively. When the LC is unidirectionally aligned by surface anchoring, GNRs also align along $\mathbf{N_0}$ and show polarization-dependent extinction color [Figs. 2(g), 2(h), and 2(i)] and extinction peaks [Fig. 2(j)].

The long-range alignment of GNRs in thermotropic LCs can be controlled by surface boundary conditions. When dispersed in unaligned LC, GNRs follow the orientation of the local LC director $\mathbf{N}$ [Fig. 3(a)], showing polarization-dependent extinction colors without any alignment [Figs. 3(b) and 3(c)]. However, when 5CB is confined into a droplet in the PDMS host, the tangentially degenerate alignment of 5CB on the surface of PDMS results in a bipolar director configuration of the 5CB droplet. Then GNRs are found following the director of a 5CB droplet and show polarization-dependent extinction colors [Figs. 3(e) and 3(f)], which depend on the alignment of nanorods within the droplet as well as on polarization changes of light traversing the birefringent LC medium within the droplet.

The long-range unidirectional alignment of comparatively larger GNRs [Fig. 4(a)] in lyotropic LC hosts can be achieved by the shearing force that sets $\mathbf{N_0}$. When the polarization of incident light $\mathbf{P}$ is parallel to $\mathbf{N_0}$, the LC with concentrated aligned GNRs in $N_C$ exhibits a transmitted-light green color while it shows a pink color for $\mathbf{P}\perp\mathbf{N_0}$ [Figs. 4(b) and 4(c)]. The Schlieren texture in a 3-$\mu$m thick cell is observed between crossed polarizers in the visible light, showing half-integer-strength disclinations in Fig. 4(d). The dark-field images obtained for two orthogonal polarizations in a sample region corresponding to the POM texture are shown in Figs. 4(e) and 4(f). The scattered light from GNRs in $N_C$ yields a green color for $\mathbf{P}\perp\mathbf{N}(\mathbf{r})$ because predominantly only the transverse SPR mode (~530 nm) is excited while the scattered light from GNRs in $N_C$ shows a red color for $\mathbf{P} \parallel \mathbf{N}(\mathbf{r})$ because mostly only the longitudinal SPR mode (~680 nm) is excited in the composite. This dependence signifies that the average nanorod orientation is parallel to $\mathbf{N}(\mathbf{r})$. The polarization-dependent scattering that arises from the excitation of SPR can be used to determine the spatial patterns of orientation of GNRs, which

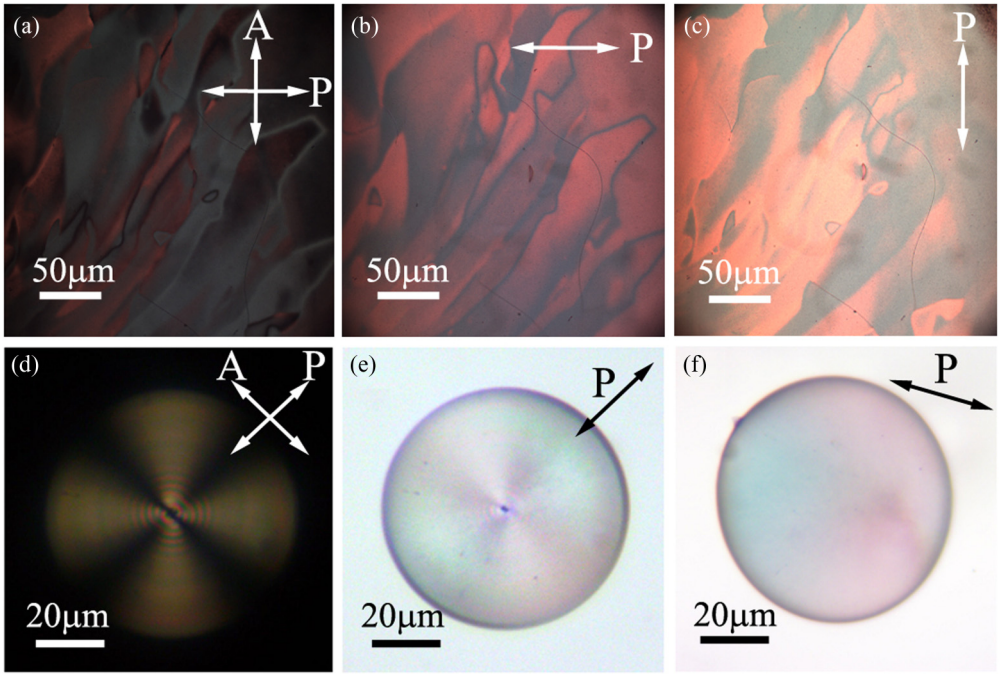


FIG. 3. (Color online) (a) POM image of an unaligned concentrated GNR-5CB composite sandwiched between two parallel glass plates. (b, c) Transmission-mode optical images of a GNRs-5CB composite under polarized light. (d) POM image of GNR-5CB droplet suspended within a PDMS matrix. (e, f) Transmission-mode optical images of GNRs-5CB droplets obtained under polarized-light illumination showing polarization-dependent colors.

match the spatial variations of the director field $\mathbf{N}(\mathbf{r})$ of $N_C$, as illustrated in Fig. 4(g).

In addition to shearing force, surface alignment by rubbing and boundary confinement set by different confinement geometries and treatment of surfaces, GNR dispersions can be aligned and controlled by light (Fig. 5). Photoalignment layers define the surface boundary conditions for **N** parallel to their azobenzene groups that orient orthogonally to the

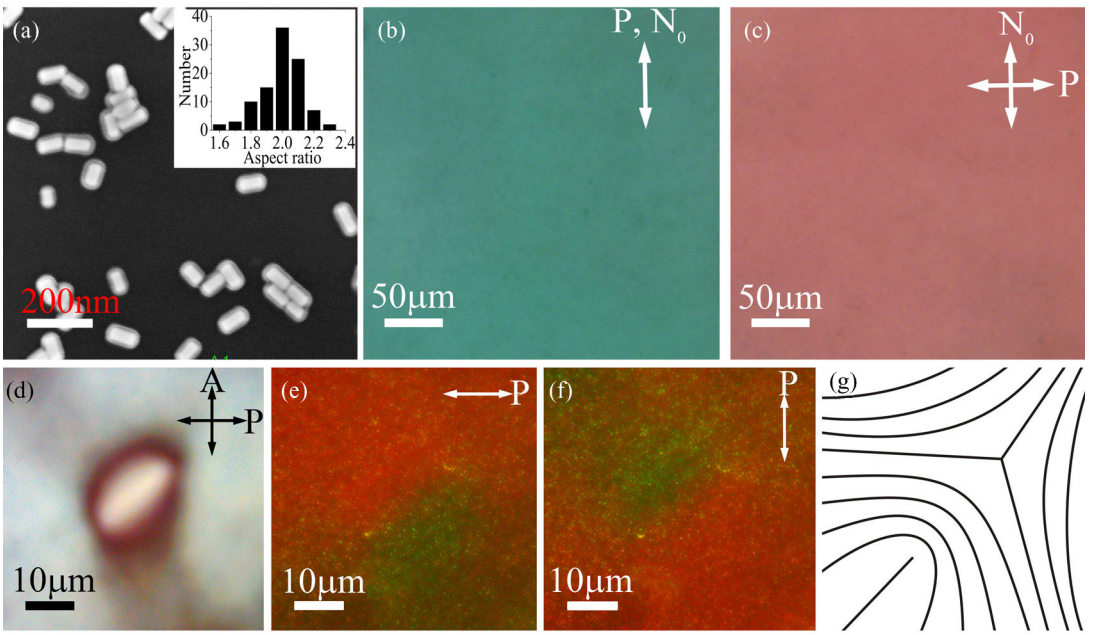


FIG. 4. (Color online) (a) SEM image of mPEG-functionalized GNRs. The inset of (a) shows the distribution of aspect ratios of used GNRs. (b, c) Transmission-mode optical microscopy micrographs of GNRs in aligned $N_C$ with the polarization of incident light (b) parallel and (c) perpendicular to the far-field director $\mathbf{N_0}$. (d) POM image showing half-integer disclination defects in unaligned samples of the dispersions of GNRs in $N_C$. (e, f) Polarized dark-field images of the same area as shown in (d) obtained for two orthogonal polarizations denoted by white double arrows. (g) A schematic of the director field $\mathbf{N}(\mathbf{r})$ corresponding to (d–e).

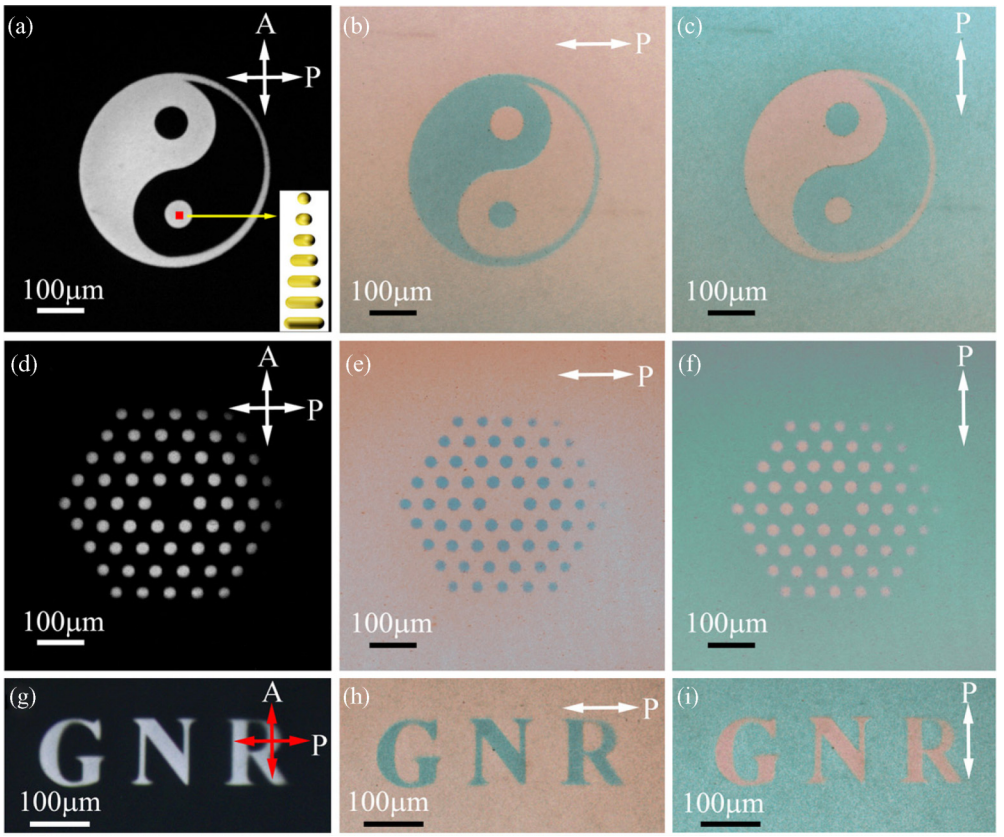


FIG. 5. (Color online) (a) A POM micrograph of a "yin-yang"-shaped twist domain within a uniformly aligned cell with GNRs-5CB obtained by patterned illumination of the photoalignment layer. (b, c) The corresponding brightfield micrographs for polarizations of incident light (b) perpendicular and (c) parallel to **N**. (d) POM and (e, f) brightfield micrographs of a hexagonal pattern created by patterned illumination. (g) POM and (h, i) brightfield optical micrographs of a twisted "GNR" pattern created by spatially varying illumination. Inset in (a) depicts the $\pi/2$ twist of **N** and GNRs across the cell thickness within twist domains.

linear polarization of the patterning blue-light illumination. This allows one to first align the composite unidirectionally and then induce $\pi/2$-twist domains with GNRs following **N**, as guided by polarized illumination patterns. In our cells, light propagation within twisted domains satisfies the so-called Mauguin condition [37]. Therefore, the traversing light's linear polarization direction also follows the rotation of **N**. Consequently, longitudinal and transverse SPRs of aligned nanorods can be selectively excited, as determined by mutual orientations of **N** and the linear polarization of incident light (Fig. 5). When viewed in polarized white light, the twisted and nontwisted areas exhibit different colors due to selective excitation of the different SPR modes. Anisotropic GNR orientations and perceived colors can be tuned dynamically through defining boundary conditions at one or both confining plates, depending on the need.

### B. Nanoparticle size- and shape-dependent optical properties of composites

The LC-aligned GNRs at high concentrations give rise to large absorption anisotropy and the reversal of the sign of birefringence (Fig. 6), which is distinctly different from that of randomly dispersed GNRs in water [38]. The absorption anisotropy ("dichroism") for single nonspherical metallic nanopaticle arises from the shape dependence of SPR. When GNRs are aligned in LCs, the collective excitation of SPRs is strongly polarized. The polarization-dependent extinction coefficients ($\alpha^{\rm ext}_{\parallel,\perp}$) of GNRs in lyotropic $N_C$ are calculated by characterizing the transmitted spectra $\alpha^{\rm ext}_{\parallel,\perp} = -\ln T_{\parallel,\perp}/d$, where $T_\parallel$ and $T_\perp$ are the transmittances of the sample at $\mathbf{P}||\mathbf{N_0}$ and $\mathbf{P}\perp\mathbf{N_0}$, respectively [Figs. 6(a) and 6(b)], and $d$ is the thickness of the sample. The extinction coefficients are comprised of the contributions due to the absorption and scattering of GNRs, i.e., $\alpha^{\rm ext}_{\parallel,\perp} = \alpha^{\rm abs}_{\parallel,\perp} + \alpha^{\rm scat}_{\parallel,\perp}$, where $\alpha^{\rm abs}_{\parallel,\perp}$ and $\alpha^{\rm scat}_{\parallel,\perp}$ are absorption and scattering coefficients of the GNR-LC composites, respectively. The longitudinal SPR peak, molar absorption, and scattering coefficients are highly aspect ratio- and size-dependent [39]. First, the longitudinal SPR peak red-shifts and depends on the aspect ratio of GNR linearly at a fixed effective volume, while the longitudinal SPR peak also red-shifts by increasing the effective volume at a fixed aspect ratio. Second, the molar extinction coefficient increases rapidly with the effective volume [33]. For example, the extinction cross section for the longitudinal SPR mode ($\sigma^{\rm ext}_\parallel$) of GNRs of 20 nm in diameter and 50-nm long is $2.0 \times 10^{-11}$ cm$^2$, while this value increases dramatically to $4.3 \times 10^{-10}$ cm$^2$ for GNRs of 40 nm in diameter and 73 nm in length. The ratio of the volume of these two sizes of GNRs is ~6, while that of $\sigma^{\rm ext}_\parallel$ is more than 20. So the advantage of large GNRs is that they provide a means of achieving strong extinction

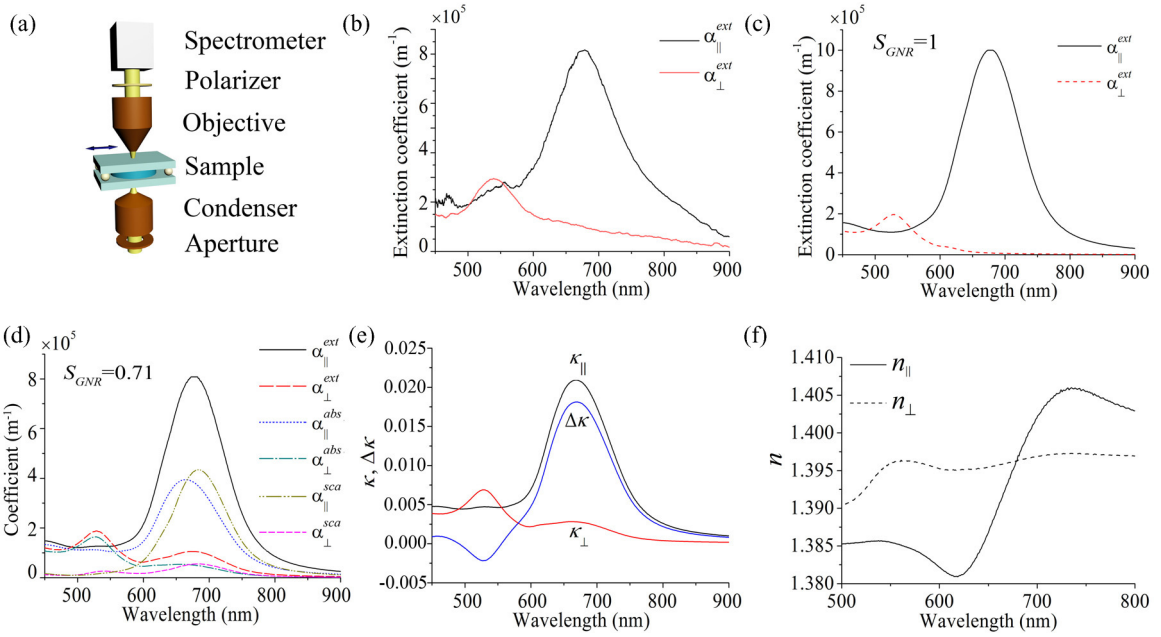


FIG. 6. (Color online) (a) A schematic of the setup used to measure the polarization-dependent transmitted spectra; the arrow indicates orientation of $\mathbf{N_0}$ set by the shear force. (b) Experimental extinction spectra of GNRs in $N_C$ at $4.7 \times 10^{-8}$ M. (c) Simulated extinction coefficients for the same concentration of GNRs in $N_C$ as (b) for two orthogonal polarizations of incident light and for $S_{\mathrm{GNR}} = 1$. (d) Computer-simulated spectral dependencies of extinction, absorption, and scattering coefficients for two orthogonal polarizations of incident light for $S_{\mathrm{GNR}} = 0.71$. (e) Calculated imaginary parts of refractive indices and its anisotropy. (f) Calculated spectral dependence of effective-medium refractive indices $n_{\parallel}$ and $n_{\perp}$.

at much lower concentrations or volume fractions of large GNRs. Third, the relative contribution of scattering to the total extinction ($\sigma_{\parallel}^{\mathrm{abs}}/\sigma_{\parallel}^{\mathrm{ext}}$) increases with increasing the effective volume of GNRs. For example, this ratio of GNRs of 20 nm in diameter and 50-nm long is ~12%, while it increases to ~52% for GNRs of 40 nm in diameter and 73 nm in length. This property makes dispersions of large GNRs good candidates for applications based on light scattering.

The quality of orientational ordering of GNRs in LC can be characterized by the scalar order parameter defined as $S_{\mathrm{GNR}} = \langle P_2(\cos\theta)\rangle$, where $P_2(x)$ is the second Legendre polynomial and $\theta$ is the angle between the long axis of a nanorod and $\mathbf{N}$. It can be estimated using the extinction anisotropy as the extinction spectra (500–800 nm) near the longitudinal SPR peak of GNRs in $N_C$ have the same shape for two orthogonal polarizations in Fig. 6(b) and the dispersion of refractive indices $n_{||}$, $n_{\perp}$ [Fig. 6(f)] within the extinction band is small. The scalar order parameter can be calculated as $S_{\mathrm{GNR}} = (\alpha_{\parallel}^{\mathrm{ext}} - \alpha_{\perp}^{\mathrm{ext}})/(\alpha_{\parallel}^{\mathrm{ext}} + 2\alpha_{\perp}^{\mathrm{ext}})$ [37]. By using $\alpha_{\parallel}^{\mathrm{ext}}$ and $\alpha_{\perp}^{\mathrm{ext}}$ at the wavelength of the longitudinal SPR peak, we obtain $S_{\mathrm{GNR}} = 0.71 \pm 0.01$.

The finite-difference time-domain (FDTD) method is used to calculate the optical properties (resonant frequencies and extinction) for aligned GNRs. The time-dependent Maxwell's equations in partial differential form are discretized using central-difference approximations in time and space. GNRs are modeled as cylinders with two semispherical caps. The optical constant of gold was taken from Ref. [40] and the average refractive index of surrounding pristine $N_C$ LC was set as $\bar{n} \approx n_{\mathrm{iso}} = 1.39$ (room temperature), which is justified by the fact that the birefringence of nematic lyotropic LCs is very low ($|\Delta n| < 0.006$). The resulting finite-difference equations are then solved using the FDTD Solutions software (from Lumerical Solutions Inc.). The extinction cross sections for two orthogonal polarizations are calculated and converted to extinction coefficients according to $\alpha_{\parallel,\perp}^{\mathrm{ext}} = \sigma_{\parallel,\perp}^{\mathrm{ext}}\eta$, where $\eta$ is the number density of GNRs ($2.8 \times 10^{13}$ mL$^{-1}$). The scattering and absorption coefficients can be calculated in a similar way. The simulated extinction coefficient spectra in Fig. 6(c) take into account the size distribution of GNRs, which is determined from scanning electron microscopy (SEM) images [inset of Fig. 4(a)]. The simulated results in Fig. 6(c) correspond to the case of a perfect orientational order of GNRs with $S_{\mathrm{GNR}} = 1$. For experimental results with $S_{\mathrm{GNR}} = 0.71$, the extinction, absorption and scattering coefficients can be calculated using equations $\alpha_{\parallel} = \frac{2}{3}\eta(\sigma_{\parallel} - \sigma_{\perp})S_{\mathrm{GNR}} + \frac{1}{3}\eta(\sigma_{\parallel} + 2\sigma_{\perp})$ and $\alpha_{\perp} = -\frac{1}{3}\eta(\sigma_{\parallel} - \sigma_{\perp})S_{\mathrm{GNR}} + \frac{1}{3}\eta(\sigma_{\parallel} + 2\sigma_{\perp})$ [Fig. 6(d)] [41,42], where $\alpha_{\parallel}$ and $\alpha_{\perp}$ denote extinction, absorption, and scattering coefficients for the two orthogonal polarizations at longitudinal SPR wavelength, and $\sigma_{\parallel}$ and $\sigma_{\perp}$ are the corresponding calculated extinction, absorption, and scattering cross sections of pure longitudinal and transverse SPR modes of GNRs.

The complex effective-medium refractive index $\tilde{n} = n + i\kappa$ of our nanostructured composite system can be calculated using the simulated polarization-sensitive absorption coefficients $\alpha_{\parallel}^{\mathrm{abs}}$ ($\mathbf{P}||\mathbf{N_0}$) and $\alpha_{\perp}^{\mathrm{abs}}$ ($\mathbf{P}\perp\mathbf{N_0}$). The imaginary parts of refractive index $\kappa_{||}$ and $\kappa_{\perp}$ are calculated as $\kappa_{\parallel,\perp} = \alpha_{\parallel,\perp}^{\mathrm{abs}}\lambda/4\pi$ and the dispersion of the extinction anisotropy ($\Delta\kappa = \kappa_{||} - \kappa_{\perp}$) is shown in Fig. 6(e) [42]. The dispersion of the refractive indices $n_{||}$ ($\mathbf{P}||\mathbf{N_0}$) and $n_{\perp}$ ($\mathbf{P}\perp\mathbf{N_0}$) can be determined according to the Kramers-Krönig relations using

the absorption coefficient $\alpha^{\rm abs}_{\parallel,\perp}$ in Fig. 6(d): $n_{\parallel,\perp}(\lambda) = n^{\rm offset}_{\parallel,\perp} = [1/(2\pi^2)]\,{\rm P.V.}\int_{\lambda_1}^{\lambda_2} \alpha^{\rm abs}_{\parallel,\perp}(\lambda)/[1-(\lambda'/\lambda)^2]d\lambda'$, where P.V. is the Cauchy principal value of the integral. The integration ranges from $\lambda_1 = 450$ nm to $\lambda_2 = 900$ nm. The used values of offset extraordinary and ordinary indices $n^{\rm offset}_{\parallel,\perp}$ are based on $\bar{n}_{\rm LC} = 1.39$ and the intrinsic optical anisotropy $\Delta n_{\rm LC} = -0.006 \pm 0.001$ of the $N_C$. The effective-medium optical anisotropy of the GNRs-$N_C$ composite is much larger than the intrinsic birefringence of $N_C$ and changes sign at around the longitudinal SPR peak wavelength [Fig. 6(f)].

## IV. DISCUSSION

### A. Strong anchoring and elastic alignment

In general, the alignment of rod-like or other nonspherical particles dispersed in the nematic LC could be caused by GNR-LC matrix interaction in "strong," "weak," or finite surface anchoring regimes. In the strong anchoring regime, the GNR-matrix interaction is expected to be mediated mostly by the minimization of elastic free energy due to director distortions induced by nanoparticles while having the director at LC-GNR surfaces follow the tangential boundary conditions [21]. In contrast, in the regime of weak surface anchoring, the director distortions in the LC bulk and energetic cost due to them can be neglected as the director meets the GNR-LC surface at different angles, so that the anisotropic nanoparticle orientation is determined by minimization of the surface anchoring cost due to the deviation of the director from the tangential easy axis orientation [20]. Although the most common situation is that of the finite anchoring regime, with both elastic and surface anchoring terms contributions to the free energy being nonnegligible, analytical modeling in this general case is difficult and, therefore, we will analyze the strong and weak anchoring limits to get insights into the physical underpinnings behind the observed alignment.

By employing electrostatic analogy, de Gennes and Brochard [21] demonstrated that cylindrical particles with strong tangential anchoring adopt equilibrium orientation along the far-field LC director at which the elastic energy is minimized. An elastic torque arises whenever the cylinder's axis orientation deviates from that along $\mathbf{N_0}$ due to the additional energetic cost of these elastic distortions. In the strong anchoring regime, this elastic torque competes with thermal fluctuations that tend to randomize the orientations of colloidal nanorods. We adopt the approach of Brochard and de Gennes [21,43] to explore the expected orientational ordering in this strong anchoring regime. In the approximation of three Frank elastic constants being equal, $K_{11} = K_{22} = K_{33} = K$ (where $K_{11}$, $K_{22}$, and $K_{33}$ are Frank elastic constants for splay, twist, and bend, respectively), the elastic free energy cost of nanorod realignment to an angle $\theta$ can be calculated as $U_{\rm elastic} = 2\pi CK\theta$, where we use the expression for "capacitance" [43] that can be applied to a rod of relatively short ratio with $L$ and $R$ being its length and radius, respectively,

$$C = 2L\sqrt{1-(R/L)^2}\left[\ln\left(\frac{1+\sqrt{1-(R/L)^2}}{1-\sqrt{1-(R/L)^2}}\right)\right]^{-1}.$$

The equilibrium distribution of GNR orientations due to the competition between thermal fluctuation and elastic interactions with the LC host medium follows Boltzmann statistics: $f_e(\theta) \propto \exp(-\xi\theta^2)$, where $\xi = 2\pi CK/(k_{\rm B}T)$, $k_{\rm B}$ is the Boltzmann constant and $T$ is temperature. Thus, the scalar orientational order parameter is $S_{\rm GNR} = \int_0^{\pi} P_2(\cos\theta) f_e(\theta)\sin\theta d\theta$. For typical $K = 1$–$10$ pN for lyotropic LC [44], $T \approx 300$ K and the average size of GNRs, we find that elastic energy $U_{\rm elastic} = 3.2\times10^{-19}\theta^2 \sim 3.2\times10^{-18}\theta^2 J, \xi = 7.7\times10^1 \sim 7.7\times10^2$, and $S_{\rm GNR} = 0.981 \sim 0.998$. The elastic torque exerted on GNRs by the LC medium is $\partial U_{\rm elastic}/\partial\theta = 4\pi CK\theta = 6.4\times10^2\theta \sim 6.4\times10^3\theta\, pN\cdot$nm. These high values of theoretically estimated scalar order parameter would imply very strong elastic torques on GNRs even at very small deviations of the long axis of GNRs from the LC director, which contradicts our observations. Indeed, the experimental order parameter for our GNRs in the lyotropic LC system $S_{\rm GNR} = 0.71$ is not within the range of theoretical estimates under the strong anchoring assumption, implying that the alignment of GNRs in nematic LCs does not derive from the elastic free energy minimization due to director distortions in the strong anchoring regime. Indeed, although GNRs are relatively large, their size is still smaller than the so-called surface anchoring extrapolation length $l_e = K/W$, where W is the (polar) surface anchoring coefficient typically in the range $W = (1$–$100)\times10^{-6}$ J/m$^2$, expected to be within $l_e = 100$–$1000$ nm [45]. Furthermore, this is also consistent with the fact that rod-like and other nanoparticles in our thermotropic and lyotropic LC dispersions do not aggregate due to the minimization of elastic distortions that could be induced by these nanoparticles, but rather stay well dispersed (Figs. 2–5).

### B. Weak surface anchoring

We will show next that the self-alignment of GNRs in nematic LC can be explained by considering the "weak" surface anchoring boundary conditions and interactions of GNRs with the LC matrix via anisotropic surface anchoring interactions (i.e., alignment arises from the minimization of the surface anchoring energy due to deviation of the director at LC-GNR interfaces from that prescribed by tangential boundary conditions). This is consistent with our GNRs being smaller than $l_e$. As a result, nanorods produce only very weak elastic distortions of $\mathbf{N}$, and the director field couples only weakly to the surfaces of GNRs, so that elasticity-mediated colloidal interactions between them can be neglected and have no effects on colloidal stability. The well-defined alignment of GNRs arises from anisotropic surface anchoring interactions at LC-nanorod interfaces. Nanoparticles induce tangential boundary conditions for $\mathbf{N}$, so that the surface anchoring energy is minimized when long axes of GNRs align along $\mathbf{N}$. On the other hand, the dimensions of GNRs are still an order of magnitude larger than that of micelles, so that the continuum theories of LCs can be applied to model our experimental observations. Assuming that the polar surface anchoring energy density has Rapini-Papoular form $f_{sa} = (W/2)\sin^2\beta$ (where $\beta$ is an angle between $\mathbf{N}$ and the "easy" axis parallel to GNR's surface) [46], we find the total surface anchoring energy as the integral of the surface anchoring energy density over the surface of GNRs, which

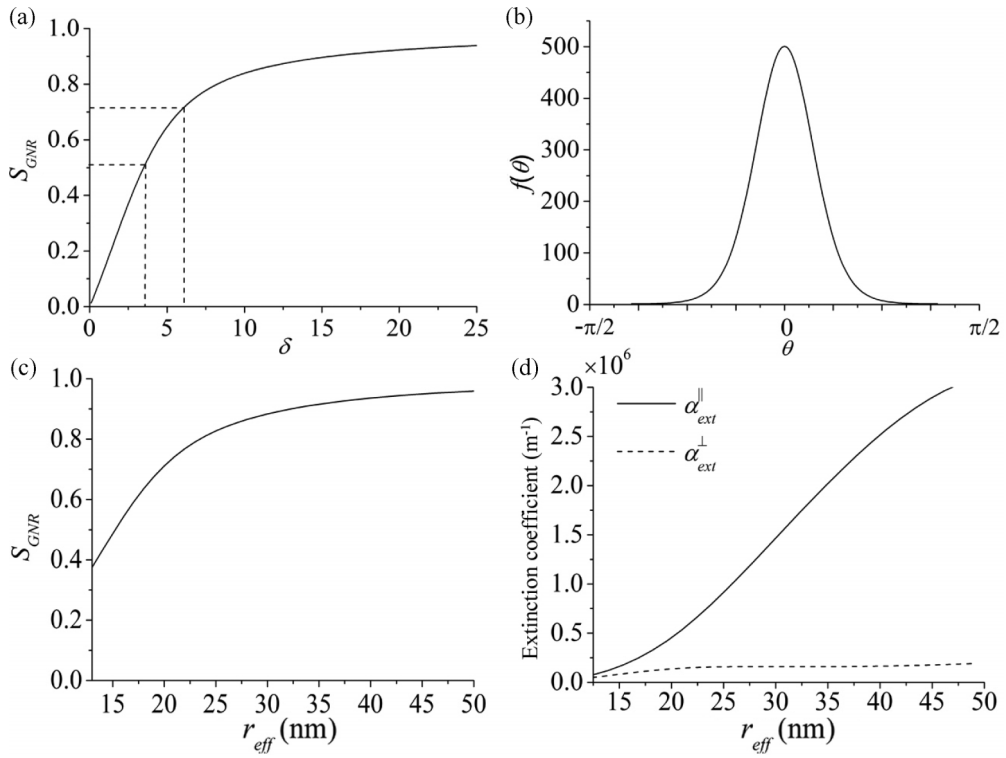


FIG. 7. (a) Order parameter $S_{\mathrm{GNR}}$ vs. $\delta = \pi LRW/(2k_BT)$. (b) Distribution of GNR orientations with respect to **N** at $S_{\mathrm{GNR}} = 0.71$. (c) Order parameter $S_{\mathrm{GNR}}$ vs. effective radius $r_{\mathrm{eff}}$ of the nanoparticle. (d) Extinction coefficients at longitudinal SPR wavelength vs. $r_{\mathrm{eff}}$.

is a function of the angle $\theta$ between **N** and the GNR's long axis. The equilibrium distribution of GNR orientations due to surface anchoring interactions follows Boltzmann statistics: $f_s(\theta) \propto \exp(-\delta \sin^2\theta)$, where $\delta = \pi LRW/(2k_BT)$. Thus, the scalar orientational order parameter reads

$$S_{\mathrm{GNR}} = \int_0^{\pi} P_2(\cos\theta) f_s(\theta) \sin\theta d\theta$$
$$= 3\exp(\delta)/[2\sqrt{\pi\delta}\,\mathrm{erf}(i\sqrt{\delta}/i)] - 3/(4\delta) - 1/2,$$

where $\mathrm{erf}(x)$ is an error function [Fig. 7(a)]. For the experimental data on dispersions of the larger GNRs in lyotropic $N_c$, $S_{\mathrm{GNR}} = 0.71$, $L \approx 73$ nm, $R \approx 20$ nm, and $T \approx 300$ K, we obtain $\delta \approx 6.0$ [Fig. 7(a)] and $W \approx 1.1 \times 10^{-5}$ J/m$^2$, which is comparable to measured values for similar LC-solid interfaces [47]. The equilibrium distribution of GNR orientations with respect to **N** calculated for $S_{\mathrm{GNR}} = 0.71$ is shown in Fig. 7(b). For the smaller GNRs dispersed in thermotropic nematic LC, $S_{\mathrm{GNR}} = 0.51$, $L \approx 50$ nm, $R \approx 10$ nm, we obtain $\delta \approx 3.6$ [Fig. 7(a)] and $W \approx 1.9 \times 10^{-5}$ J/m$^2$, which is also consistent with literature values of surface anchoring at similar LC-solid interfaces [47]. Thus, the surface anchoring mediated alignment is consistent with the experimentally studied properties of alignment of rod-like particles in both lyotropic and themotropic nematic LCs.

Using the surface-anchoring-based model, we can calculate how the order parameter of GNRs and optical properties of the LC-GNR composite vary with changing the size of the nanorods. The lower limit of the size of GNR that is appropriate to consider is set by the fact that GNRs should be much bigger than micelles or thermotropic LC molecules, so we can apply the concept of director of LC and continuum theory at this scale. The upper limit is set by the fact that GNRs of the LC-based optical effective-medium system should be much smaller than the wavelength of light in the visible part of spectrum, so that one can expect the effective-medium behavior. The size of GNRs can be expressed by the effective radius $r_{\mathrm{eff}}$, which is defined as that of a sphere of the same volume $V = 4\pi r_{\mathrm{eff}}^3/3 = \pi R^2 L$. To satisfy the above-mentioned constrains for gold nanorods, $r_{\mathrm{eff}}$ approximately falls in the range from 12 to 50 nm. The surface anchoring energy increases with increasing $r_{\mathrm{eff}}$, resulting in the increase of $S_{\mathrm{GNR}}$, as shown in Fig. 7(c). Calculated for the experimental aspect ratio of used GNRs, $S_{\mathrm{GNR}}$ increases rapidly when $r_{\mathrm{eff}}$ is relatively small, but then saturates while approaching $S_{\mathrm{GNR}} = 1$ for larger values of $r_{\mathrm{eff}}$, as shown in Fig. 7(c). In addition, the increase of $S_{\mathrm{GNR}}$ with increasing $r_{\mathrm{eff}}$ gives rise to the increase of anisotropy of the extinction coefficient of GNRs, as shown by plotting $\alpha_{\mathrm{ext}}^{\parallel}$ and $\alpha_{\mathrm{ext}}^{\perp}$ versus $r_{\mathrm{eff}}$ in Fig. 7(d). As one can see, it is beneficial to use larger GNRs to achieve higher order parameter and larger optical extinction anisotropy. We note, however, that although the anchoring-mediated GNR-LC interactions play a dominant role, there may be a contribution due to weak elastic distortions as well. Furthermore, our estimates above utilize a number of approximations and assumptions, such as the use of the Rapini-Papoular potential even for large angles between the easy axis and the director. It will be, therefore, of strong interest to further understanding of self-alignment behavior in this composite soft matter system by means of numerical modeling.

## V. CONCLUSION

In summary, we have demonstrated the shape-dependent dispersion and alignment of nonaggregating plasmonic gold nanoparticles in lyotropic and thermotropic nematic LCs. Shape-isotropic nanoparticles could disperse in nematic LC without alignment while GNRs show unidirectional oriented self-assembly at high concentration in a nematic LC host. This self-assembly at high GNR concentrations gives rise to strong polarization-dependent absorption and scattering, abnormal dispersions of refractive index, and enhanced optical birefringence with sign reversal in the spectral vicinity of the longitudinal SPR peak. A phenomenological model based on the anisotropic surface interaction explains the unidirectional alignment of larger GNRs in the LC host. We showed that the use of GNRs allows one to achieve higher order parameter values, larger optical extinction, as well as extinction anisotropy and modifications of the effective medium indices as compared to the pristine LC, as long as the size of GNRs is less than $\lambda/10$ to exhibit effective medium behavior. Our findings may enable fabrication of novel LC optical devices based on liquid crystals and nanomaterials, such as plasmonic polarizers, displays, and various electro-optical elements. On the other hand, from the fundamental standpoint of view, nonaggregating colloidal dispersions of complex-shaped nanoparticles in LCs may lead to the formation of new types of mesophases with unusual combinations of orientational and partial positional ordering.

## ACKNOWLEDGMENTS

This research was supported by the US Department of Energy, Office of Basic Energy Sciences, Division of Materials Sciences and Engineering under Award ER46921 (Q.L., Y.Z., A.M., I.I.S.) and partially by an NSF Grant No. DGE-0801680 (A.M., I.I.S.). We thank Michael Campbell, Nan Wang, Julian Evans, Pengxin Chen, Noel Clark, Leo Radzihovsky, Yalun Wang, Qiuqiang Zhan, and Jun Qian for discussions.

[1] I. Muševič, M. Škarabot, and M. Humar, J. Phys. Condens. Matter **23**, 284112 (2011).
[2] B. Senyuk, Q. Liu, S. He, R. D. Kamien, R. B. Kusner, T. C. Lubensky, and I. I. Smalyukh, Nature (London) **493**, 200 (2013).
[3] U. Tkalec, M. Ravnik, S. Čopar, S. Žumer, and I. Muševič, Science **333**, 62 (2011).
[4] I. Muševič, M. Škarabot, U. Tkalec, M. Ravnik, and S. Žumer, Science **313**, 954 (2006).
[5] P. Poulin, H. Stark, T. C. Lubensky, and D. A. Weitz, Science **275**, 1770 (1997).
[6] J. P. F. Lagerwall and G. Scalia, Curr. Appl. Phys. **12**, 1387 (2012).
[7] C. Lapointe, T. Mason, and I. I. Smalyukh, Science **326**, 1083 (2009).
[8] M. R. Jones, K. D. Osberg, R. J. Macfarlane, M. R. Langille, and C. A. Mirkin, Chem. Rev. **111**, 3736 (2011).
[9] H. K. Bisoyi and S. Kumar, Chem. Soc. Rev. **40**, 306 (2011).
[10] J. Kao, K. Thorkelsson, P. Bai, B. J. Rancatore, and T. Xu, Chem. Soc. Rev. **42**, 2654 (2013).
[11] T. Hegmann, H. Qi, and V. M. Marx, J. Inorg. Organomet. Polym. **17**, 483 (2007).
[12] B. Senyuk, J. S. Evans, P. Ackerman, T. Lee, P. Manna, L. Vigderman, E. R. Zubarev, J. van de Lagemaat, and I. I. Smalyukh, Nano Lett. **12**, 955 (2012).
[13] B. Senyuk, N. Behabtu, B. G. Pacheco, T. Lee, G. Ceriotti, J. M. Tour, M. Pasquali, and I. I. Smalyukh, ACS Nano **6**, 8060 (2012).
[14] B. Senyuk and I. I. Smalyukh, Soft Matter **8**, 8729 (2012).
[15] R. J. Macfarlane, B. Lee, M. R. Jones, N. Harris, G. C. Schatz, and C. A. Mirkin, Science **334**, 204 (2011).
[16] M. R. Jones, R. J. Macfarlane, B. Lee, J. Zhang, K. L. Young, A. J. Senesi, and C. A. Mirkin, Nat. Mater. **9**, 913 (2010).
[17] D. F. Gardner, J. S. Evans, and I. I. Smalyukh, Mol. Cryst. Liq. Cryst. **545**, 1227 (2011).
[18] M. Mitov, C. Portet, C. Bourgerette, E. Snoeck, and M. Verelst, Nat. Mater. **1**, 229 (2002).
[19] Q. Liu, Y. Cui, D. Gardner, X. Li, S. He, and I. I. Smalyukh, Nano Lett. **10**, 1347 (2010).
[20] Q. Liu, B. Senyuk, J. Tang, T. Lee, J. Qian, S. He, and I. I. Smalyukh, Phys. Rev. Lett. **109**, 088301 (2012).
[21] F. Brochard and P.-G. de Gennes, J. Phys. (Paris) **31**, 691 (1970).
[22] B. D. Smith, D. J. Kirby, I. O. Rivera, and C. D. Keating, ACS Nano **7**, 825 (2013).
[23] L. Vigderman, B. P. Khanal, and E. R. Zubarev, Adv. Mater. **24**, 4811 (2012).
[24] G. Scalia, Chem. Phys. Chem. **11**, 333 (2010).
[25] G. Scalia, C. von Bühler, C. Hägele, S. Roth, F. Giesselmann, and J. P. F. Lagerwall, Soft Matter **4**, 570 (2008).
[26] J. P. F. Lagerwall, G. Scalia, M. Haluska, U. Dettlaff-Weglikowska, S. Roth, and F. Giesselmann, Adv. Mater. **19**, 359 (2007).
[27] I. Dierking, G. Scalia, P. Morales, and D. Leclere, Adv. Mater. **16** 865 (2004).
[28] L. M. Blinov and V. G. Cigrinov, *Electrooptic Effects in Liquid Crystal Materials* (Springer-Verlag, New York, 1996).
[29] J. Perez-Juste, L. M. Liz-Marzan, S. Carnie, D. Y. C. Chan, and P. Mulvaney, Adv. Funct. Mater. **14**, 571 (2004).
[30] S. T. Sivapalan *et al.*, J. Phys. Chem. C **117**, 10677 (2013).
[31] J. Xie, J. Y. Lee, and D. I. C. Wang, Chem. Mat. **19**, 2823 (2007).
[32] R. Bartolino, T. Chiaranza, M. Meuti, and R. Compagnoni, Phys. Rev. A **26**, 1116 (1982).
[33] Y. Hendrikx, J. Charvolin, M. Rawiso, L. Liebert, and M. C. Holmes, J. Phys. Chem. **87**, 3991 (1983).
[34] Q. Liu, C. Beier, J. Evans, T. Lee, S. He, and I. I. Smalyukh, Langmuir **27**, 7446 (2011).
[35] L. De Sio *et al.*, J. Mater. Chem. C **1**, 7483 (2013).
[36] A. Martinez, H. C. Mireles, and I. I. Smalyukh, Proc. Natl. Acad. Sci. USA **108**, 20891 (2011).
[37] B. Bahadur, *Handbook of Liquid Crystals* (Wiley-VCH, Weinheim, Germany, 1998), Vol. 2A.
[38] M. E. Stewart, C. R. Anderton, L. B. Thompson, J. Maria, S. K. Gray, J. A. Rogers, and R. G. Nuzzo, Chem. Rev. **108**, 494 (2008).

[39] P. K. Jain, K. S. Lee, I. H. El-Sayed, and M. A. El-Sayed, J. Phys. Chem. B **110**, 7238 (2006).
[40] E. D. Palik, *Handbook of Optical Constants of Solids* (Academic, New York, 1998).
[41] M. F. Islam, D. E. Milkie, C. L. Kane, A. G. Yodh, and J. M. Kikkawa, Phys. Rev. Lett. **93**, 037404 (2004).
[42] E. Charlet and E. Grelet, Phys. Rev. E **78**, 041707 (2008).
[43] C. J. Smith and C. Denniston, J. Appl. Phys. **101**, 014305 (2007).
[44] A. V. A. Pinto and L. Q. Amaral, J. Phys. Chem. **94**, 3186 (1990).
[45] P.-G. de Gennes and J. Prost, *The Physics of Liquid Crystals* (Clarendon, Oxford, 1995).
[46] P. van der Schoot, V. Popa-Nita, and S. Kralj, J. Phys. Chem. B **112**, 4512 (2008).
[47] A. M. Ribas, L. R. Evangelista, A. J. Palangana, and E. A. Oliveira, Phys. Rev. E **51**, R5204 (1995).